Lateral-torsional buckling assessment of steel beams through a stiffness reduction method

Merih Kucukler*, Leroy Gardner, Lorenzo Macorini

Department of Civil and Environmental Engineering, South Kensington Campus, Imperial College London, London, SW7 2AZ, UK

Abstract

This paper presents a stiffness reduction approach utilising Linear Buckling Analysis (LBA) with developed stiffness reduction functions for the lateral-torsional buckling (LTB) assessment of steel beams. A stiffness reduction expression is developed for the LTB assessment of beams subjected to uniform bending and modified for the consideration of moment gradient effects on the development of plasticity. The proposed stiffness reduction method considers the influence of imperfections and plasticity on the response through the reduction of the Young's modulus E and shear modulus G and obviates the need of using LTB buckling curves in design. The accuracy and practicality of the method are illustrated for regular, irregular, single and multi-span beams. In all of the considered cases, the proposed method is verified against the results obtained through nonlinear finite element modelling.

Keywords: Stiffness reduction; lateral-torsional buckling; steel beams; inelastic buckling

1. Introduction

The spread of plasticity leading to reduction in stiffness erodes the elastic buckling strengths of steel beams. In practical design, this may be accounted for by two alternative approaches: (i) use of semi-empirical design equations reducing the ultimate cross-section bending resistance through buckling reduction factors [1–5] (ii) reduction of stiffness [6–9]. Though the latter may be seen to represent the actual physical response more realistically, the former has traditionally been adopted in steel design specifications [10–12] as its applicability is well suited to hand calculations. Recently, developments in computer technology have meant that the ability to perform elastic Linear Buckling Analysis (LBA) is readily available to structural engineers. The use of stiffness reduction approaches in conjunction with LBA may now therefore offer an accurate and practical means of determining inelastic buckling capacities of steel beams. This method may also lead to more direct design in

*Corresponding author

Email addresses: merih.kucukler10@imperial.ac.uk (Merih Kucukler), leroy.gardner@imperial.ac.uk (Leroy Gardner), l.macorini@imperial.ac.uk (Lorenzo Macorini)

comparison to the traditional approaches, as the influence of moment gradient, load height, restraint type and position and the interactions between unrestrained segments of beams during buckling can be directly captured through LBA. Considering these benefits, [13–16] proposed performing the lateral-torsional buckling (LTB) assessment of steel beams through LBA where the Young's modulus E and shear modulus G are reduced on the basis of the corresponding bending moments. Wongkaew [13], Wongkaew and Chen [14] put forward stiffness reduction expressions based on the LRFD [17] LTB assessment formulae. Trahair and Hancock [16] derived stiffness reduction functions using the AS-4100 [12] LTB equations, and Trahair [18, 19] applied the approach for the LTB assessment of steel cantilever beams and monosymmetric beams. In all previous studies [13, 14, 16, 18, 19], the proposed methods were only compared against design specifications [12, 17], but not against the results from nonlinear finite element modelling, and the considered cases were not exhaustive.

Building upon this previous work, a stiffness reduction method, applied by reducing the Young's modulus E and shear modulus G through developed stiffness reduction functions and performing LBA, is proposed in the present paper. A stiffness reduction function is first derived for the LTB assessment of beams subjected to uniform bending and then modified to allow for the influence of moment gradient on the development of plasticity. Since the developed stiffness reduction functions take full account of the deleterious influence of the spread of plasticity, residual stresses and geometrical imperfections, the proposed method obviates the need to use LTB strength equations, and thus offers a practical and direct means of design. The proposed method, which can readily be applied with any software capable of providing elastic buckling moments through Linear Buckling Analysis, is also able to capture the influence of a varying degree of support afforded by connected members with the development of plasticity. The stiffness reduction method proposed herein is intended to be used in conjunction with that proposed for in-plane design in Kucukler et al. [20] within a design framework where in-plane and out-of-plane analyses of members and frames subjected to in-plane loading are performed separately.

The application and accuracy of the proposed stiffness reduction method are illustrated by means of comparisons with the results obtained through Geometrically and Materially Nonlinear Analyses with Imperfections (GMNIA) using finite element models, considering regular, irregular, single and multi-span beams. In comparison to the previously proposed approaches, a broader series of cases is considered in this study covering a wide range of I section geometries and member slendernesses.

2. Finite element modelling

In this section, finite element models are developed and validated against experimental results from the literature. The validated finite element models, which consider material and geometric nonlinearities and involve geometrical imperfections and residual stresses, are then used in the following sections to verify the proposed stiffness reduction method.

2.1. Development of finite element models

In this study, shell elements were employed to create the finite element models using the finite element analysis software Abaqus [21]. In particular, a four-node reduced integration shell element, which is designated as S4R in the Abaqus [21] element library and accounts for transverse shear deformations and finite membrane strains, was used in all numerical simulations. To consider the spread of plasticity through the depth of a cross-section accurately, 16 elements were used for each plate constituting the flanges and web of an I section. The web plate was offset considering the thickness of the flanges so that overlapping of the flange and web plates was avoided. In the longitudinal direction of the beam models, 100 elements were used when the length to depth ratio was smaller than 20, while 200 elements were used when this value was exceeded. The fillets were incorporated into the finite element models through additional beam elements placed at the centroids of the flanges so that the section properties given in steel section tables were achieved. The default Simpson integration method was used, with five integration points through the thickness of each element. The Poisson's ratio was taken as 0.3 in the elastic range and 0.5 in the plastic range by defining the effective Poisson's ratio as 0.5 to allow for the change of cross-sectional area under load. The adopted material model used the tri-linear stress-strain relationship shown in Fig. 1, where E is the Young's modulus, E_{sh} is the strain hardening modulus, f_y and ϵ_y are the yield stress and strain respectively and ϵ_{sh} is the strain value at which the strain hardening commences. The parameters f_u and ϵ_u correspond to the ultimate stress and strain values respectively. E_{sh} was assumed to be 2 % of E and ϵ_{sh} was taken as $10\epsilon_y$, conforming to the ECCS recommendations [22]. In the finite element models, isotropic strain hardening and the von Mises yield criterion with the associated flow rule were employed. Since the constitutive formulations of Abaqus [21] adopt the Cauchy (true) stress-strain assumption, the engineering stress-strain relationship shown in Fig. 1 was transformed to the true stress-strain relationship. In all simulations, S235 steel was considered. The load-displacement response of the finite element models was determined by means of the modified Riks method [21, 23, 24], using the default convergence criteria recommended by Abaqus [21].

The residual stress patterns recommended by ECCS [22], which are displayed in Fig. 2, were applied to the finite element models. Unless otherwise indicated, the initial geometrical imperfections were assumed to be the lowest global buckling mode of a member in shape, which included twist, and 1/1000 of the laterally unrestrained member length in magnitude [25]. Since the cross-sections of all the considered beams were non-slender under pure bending based on the criteria given in EN 1993-1-1 [10], local buckling effects were not considered to be important and local imperfections were not included in the finite element models. Fork-end support conditions allowing for warping deformations and rotations, but restraining translations and twists, were adopted through defining coupling constraint relationships at the supports.

2.2. Validation of finite element models

Since this study focuses on the LTB strengths of steel beams, the experiments carried out by Dux and Kitipornchai [26] to investigate out-of-plane instability effects in steel beams of different lengths and subjected to a variety of moment gradient shapes, were chosen to validate the finite element models. In the experiments, the specimens, made up of UB 254x146 universal beam sections, were subjected to point loads along the span, while torsional and lateral restraints were provided at the points of load application. The material properties and cross-section dimensions reported by [26] for each specimen were used within the finite element models. Moreover, the measured values of geometrical imperfections (lateral bow and initial twist) provided by [26] were incorporated into the finite element models assuming them as a half-sine wave in shape for each laterally unrestrained span. The comparison between the strengths determined through GMNIA and those obtained in the experiments is shown in Table 1, where L is the length of the specimen, $\overline{\lambda}_{LT}$ is the LTB slenderness, $M_{ult,exp}$ is the ultimate experimental bending strength, $M_{ult,FE}$ is the ultimate FE bending strength, and $M_{y,pl} = W_{pl,y} f_y$ is the plastic bending moment resistance equal to the plastic section modulus $W_{pl,y}$ multiplied by the yield stress f_y. Note that the LTB slenderness $\overline{\lambda}_{LT}$ was determined as $\overline{\lambda}_{LT} = \sqrt{M_{y,pl}/M_{cr}}$ where M_{cr} is the elastic lateral-torsional buckling moment of the beam. Table 1 shows that the agreement between the ultimate strengths determined through the finite element models and those observed in the experiments is good for all considered moment gradient shapes, indicating that the finite element models are able to replicate the response of steel beams influenced by out-of-plane instability effects.

3. Stiffness reduction for lateral-torsional buckling of beams

This section addresses the derivation of a stiffness reduction function for the lateral-torsional buckling (LTB) assessment of beams. The influence of moment gradient on the stiffness reduction is also investigated.

3.1. Stiffness reduction function for lateral-torsional buckling of beams

In Kucukler et al. [20], a stiffness reduction function for the flexural buckling assessment of columns was developed through the European column buckling curves given in EN 1993-1-1 [10]. Similar to that for flexural buckling, a stiffness reduction function for LTB can be derived using the EN 1993-1-1 [10] instability assessment formulae for beams. However, recent studies [27–29] have identified inaccuracies in the two sets of LTB curves provided in EN 1993-1-1 [10]. The first is given in Clause 6.3.2.2 and may be applied to beams with any cross-section type, which will henceforth be referred to as the general case LTB equation, and the second is given in Clause 6.3.2.3 and applies principally to I sections; the latter will henceforth be referred to as the specific case LTB equation. To address identified accuracies, a Perry-Robertson equation, mechanically consistent with the LTB behaviour of beams, was proposed by Stangenberg [28] and calibrated by Taras and Greiner [29]. Although accurate and mechanically consistent, the LTB equation of [28, 29] does not lend itself to the derivation of a compact stiffness reduction function. Hence, in the present paper, to obtain a stiffness reduction function that is both accurate and compact, the LTB equation of [28, 29] is modified and re-calibrated.

3.1.1. Modification of the Perry-Robertson equation for LTB

The Perry-Robertson form of equation proposed by [28, 29] is provided in eq. (1) where η_{LT} is the generalised imperfection factor, χ_{LT} is the buckling reduction factor and $\overline{\lambda}_z$ is the non-dimensional slendernesses for flexural buckling. The flexural buckling slenderness $\overline{\lambda}_z$ can be calculated through $\overline{\lambda}_z = \sqrt{N_{pl}/N_{cr,z}}$ where $N_{cr,z}$ is the elastic flexural buckling load about the minor axis and $N_{pl} = Af_y$ is the yield load equal to the cross-sectional area A multiplied by the yield stress. Note that the LTB strength of a beam with Class 1 or 2 cross-section $M_{b,Rd}$ is determined by multiplying χ_{LT} with the plastic bending moment capacity $M_{y,pl}$, $M_{b,Rd} = \chi_{LT} M_{y,pl}$.

$$\chi_{LT} = \frac{1}{\phi_{LT} + \sqrt{\phi_{LT}^2 - \overline{\lambda}_{LT}^2}} \quad where \quad \phi_{LT} = 0.5\left[1 + \frac{\overline{\lambda}_{LT}^2}{\overline{\lambda}_z^2}\eta_{LT} + \overline{\lambda}_{LT}^2\right] \tag{1}$$

The $\overline{\lambda}_{LT}^2/\overline{\lambda}_z^2$ term, which modifies the generalised imperfection factor η_{LT}, is a key parameter for the representation of the LTB response of a beam and enables an accurate calibration of eq. (1) to GMNIA results. This parameter can be expressed as a function of $\overline{\lambda}_{LT}$, as shown in eq. (2), where $W_{pl,y}$ is the plastic section modulus about the major axis, G is the shear modulus, and I_t, I_w and I_z are the torsion and warping constants and second moment of area about the minor axis respectively.

$$\frac{\overline{\lambda}_{LT}^2}{\overline{\lambda}_z^2} = \frac{W_{pl,y}/A}{\frac{GI_t}{M_{y,pl}}\frac{\overline{\lambda}_{LT}^2}{2} + \sqrt{\left(\frac{GI_t}{M_{y,pl}}\frac{\overline{\lambda}_{LT}^2}{2}\right)^2 + I_w/I_z}} \tag{2}$$

To derive a stiffness reduction function, eq. (1) must be expressed in terms of $\overline{\lambda}_{LT}$ as described in the Section 3.1.3. However, a closed form expression of eq. (1) in terms of $\overline{\lambda}_{LT}$ cannot be obtained due to the $\overline{\lambda}_{LT}$ term in the square root, within the expression for $\overline{\lambda}_{LT}^2/\overline{\lambda}_z^2$ - see eq. (2). Thus, in this study, in order to capture the general influence of $\overline{\lambda}_{LT}^2/\overline{\lambda}_z^2$, its value for $\overline{\lambda}_{LT} = 0.5$, as shown in eq. (3), is used in eq. (1). Henceforth, this value will be denoted by κ. Although using κ in lieu of the full expression does not enable the consideration of the change of $\overline{\lambda}_{LT}^2/\overline{\lambda}_z^2$ with the length, it allows its variation with the cross-section properties influencing the LTB behaviour to be taken into account, which is necessary for the accurate calibration of eq. (1) to GMNIA results.

$$\kappa = \frac{W_{pl,y}/A}{\frac{GI_t}{8M_{y,pl}} + \sqrt{\left(\frac{GI_t}{8M_{y,pl}}\right)^2 + I_w/I_z}} \tag{3}$$

With increasing of LTB slenderness $\overline{\lambda}_{LT}$, the use of κ in eq. (1) results in smaller values of χ_{LT} compared to those obtained with the full expression for $\overline{\lambda}_{LT}^2/\overline{\lambda}_z^2$, since κ becomes much larger than $\overline{\lambda}_{LT}^2/\overline{\lambda}_z^2$. To alleviate this conservatism, a modification factor β is incorporated into eq. (1), which is similar to the approach adopted in the development of the specific case equation of Eurocode 3 [30]. With this modification and use of κ in lieu of $\overline{\lambda}_{LT}^2/\overline{\lambda}_z^2$, eq. (1) transforms to the form shown in eq. (4).

$$\chi_{LT} = \frac{1}{\phi_{LT} + \sqrt{\phi_{LT}^2 - \beta\overline{\lambda}_{LT}^2}} \quad where \quad \phi_{LT} = 0.5\left[1 + \kappa\eta_{LT} + \beta\overline{\lambda}_{LT}^2\right] \tag{4}$$

3.1.2. Calibration of the modified Perry-Robertson equation for LTB

Similar to the approach followed by [29], the modified LTB equation given in eq. (4) is calibrated by comparing the generalised imperfection factor η_{LT} to those obtained in this paper through FE modelling $\eta_{LT,FE}$. To obtain the $\eta_{LT,FE}$ values, eq. (4) is re-arranged in terms of η_{LT} to give eq. (5), where $\chi_{LT,FE}$ is the ratio of the strength determined through GMNIA to the plastic bending moment capacity $M_{y,pl}$.

$$\eta_{LT,FE} = \frac{1 - \chi_{LT,FE}}{\chi_{LT,FE}}\left(1 - \beta\chi_{LT,FE}\overline{\lambda}_{LT}^2\right)\frac{1}{\kappa} \tag{5}$$

Using eq. (5), eq. (4) was calibrated to GMNIA results for a series of fork-end supported beams subjected to uniform bending moment. In total, 30 European section shapes including IPE and HE sections were considered. The ranges of the properties of the sections are provided in Table 2, where h and b are the depth and width of the cross-section, and t_w and t_f are the web and flange thickness respectively. Ten beams were analysed for each section within the slenderness range $0.2 \leq \overline{\lambda}_{LT} \leq 2.0$, with increments in $\overline{\lambda}_{LT}$ of 0.2. As proposed by Taras and Greiner [29], the multiplication of η_{LT} by an additional cross-section factor $\sqrt{W_{el,y}/W_{el,z}}$, where $W_{el,y}$ and $W_{el,z}$ are the elastic section moduli about the major and minor axis respectively, leads to a more accurate calibration, which is also adopted in this study. After this improvement and taking β equal to 0.8, the accuracy of the proposed calibrated expressions of η_{LT} in comparison to $\eta_{LT,FE}$ values is shown in Fig. 3, where it may be seen that the proposals lead to high accuracy. β was taken as equal to 0.8 as this value resulted in the smallest coefficient of variation (COV) value of the ratios between η_{LT} and $\eta_{LT,FE}$ for the considered sections. Note that $\eta_{LT,FE}$ values become negative for some members, indicating that the strengths exceed the elastic buckling moments. This trend occurs for cross-sections with large torsional stiffnesses at high slendernesses, where beams exhibit some post-buckling strength, though this is not of real significance as the length to cross-section depth ratios of these beams lie beyond the range likely to be used in practice. The proposed equation for the LTB assessment of beams is shown in eq. (6) and the calibrated values of α_{LT}, β and $\overline{\lambda}_{LT,0}$ are provided in Table 3. In eq. (6), the limiting slenderness value $\overline{\lambda}_{LT,0}$, below which the strength of a beam is not reduced for LTB, was taken as 0.2, as the results from GMNIA do not suggest the safe adoption of a larger value. It is acknowledged however that tests [31] have indicated that a higher value may be acceptable.

$$\chi_{LT} = \frac{1}{\phi_{LT} + \sqrt{\phi_{LT}^2 - \beta\overline{\lambda}_{LT}^2}} \quad but \quad \chi_{LT} \leq 1/\overline{\lambda}_{LT}^2$$
$$where \quad \phi_{LT} = 0.5\left[1 + \kappa\alpha_{LT}(\overline{\lambda}_{LT} - \overline{\lambda}_{LT,0}) + \beta\overline{\lambda}_{LT}^2\right] \tag{6}$$

The comparison of LTB strengths determined through the calibrated LTB formula given in eq. (6) and the Eurocode 3 [10] general and specific case LTB equations with those obtained through GMNIA is set out in Table 4 where N is the number of considered beams, and S is the ratio of the LTB strength of a beam calculated through the considered formula to that determined through GMNIA. S_{av} and S_{cov} is the average and coefficient of variation (COV) of S, and S_{max} and S_{min} are the maximum and minimum values of S. Note that the results of beams with length to depth ratios between 3 and 50 (3≤L/h≤50) are included in Table 4, where it is seen that eq. (6) brings improved accuracy in comparison to both the Eurocode 3 [10] general and specific case LTB formulae.

3.1.3. Derivation of a stiffness reduction function for lateral-torsional buckling of beams

The inelastic critical buckling moment $M_{cr,i}$ of a fork-end supported beam subjected to uniform bending may be expressed by eq. (7); where $(EI_z)_r, (GI_t)_r$ and $(EI_w)_r$ are the reduced minor axis flexural stiffness, torsional stiffness and warping stiffness due to plasticity respectively, and L is the length of the beam. Trahair and Kitipornchai [9] demonstrated that, in reality, these stiffnesses (EI_z, GI_t and EI_w) reduce at different rates. However, for the sake of simplicity, the same reduction rate was considered in this study, reducing the Young's modulus E and shear modulus G through τ_{LT} as shown in eq. (8).

$$M_{cr,i} = \sqrt{\frac{\pi^2 (EI_z)_r}{L^2} \left\{ (GI_t)_r + \frac{\pi^2 (EI_w)_r}{L^2} \right\}} \tag{7}$$

$$M_{cr,i} = \tau_{LT} \sqrt{\frac{\pi^2 EI_z}{L^2} \left[GI_t + \frac{\pi^2 EI_w}{L^2} \right]} \tag{8}$$

Since the same reduction rate is applied to all stiffnesses, the inelastic buckling moment $M_{cr,i}$ can be expressed by multiplying the stiffness reduction factor τ_{LT} with the elastic buckling moment M_{cr}, as shown in Fig. 4, where $M_{y,Ed}$ is the applied bending moment. A stiffness reduction function for LTB τ_{LT} can be calculated by considering the inelastic and elastic buckling moments and applying eq. (9).

$$\tau_{LT} = \frac{M_{cr,i}}{M_{cr}} = \frac{\chi_{LT} M_{y,pl}}{M_{cr}} = \chi_{LT} \overline{\lambda}_{LT}^2 \tag{9}$$

The calibrated LTB equation given in eq. (6) is used herein to obtain χ_{LT}. Eq. (6) can be rearranged in terms of $\overline{\lambda}_{LT}$ as shown in eq. (10).

$$\overline{\lambda}_{LT}^2 = \frac{4\psi_{LT}^2}{\kappa^2 \alpha_{LT}^2 \chi_{LT}^2 \left[1 + \sqrt{1 - 4\beta\psi_{LT} \frac{\chi_{LT} - 1}{\kappa^2 \alpha_{LT}^2 \chi_{LT}}} \right]^2}$$
$$where \quad \psi_{LT} = 1 + \overline{\lambda}_{LT,0} \kappa \alpha_{LT} \chi_{LT} - \chi_{LT} \tag{10}$$

Substituting eq. (10) into eq. (9) and with $\chi_{LT} = M_{y,Ed}/M_{y,pl}$ provides eq. (11), where τ_{LT} is expressed as a function of the ratio of $M_{y,Ed}$ to $M_{y,pl}$ as well as the imperfection factor α_{LT}. The inclusion of α_{LT} in the expression of τ_{LT} enables the consideration of geometrical imperfections and residual stresses. The proposed values of α_{LT}, β, $\overline{\lambda}_{LT,0}$ and κ are provided in Table 3. The resulting stiffness reduction for different cross-section shapes is illustrated in Fig. 5, showing that the rate of stiffness reduction increases with the susceptibility of a cross-section to LTB. The derived stiffness reduction function given by eq. (11) provides exactly the same LTB strength predictions as those obtained using eq. (6). Thus, its level of accuracy is the same as that given for eq. (6) in Table 4. Note that instead of α_{LT}, β, $\overline{\lambda}_{LT,0}$ and κ values proposed in this study, those given in Table 3 for the Eurocode 3 [10] specific and general case LTB equations could also be used in eq. (11) to obtain the same LTB strength predictions determined through the Eurocode 3 [10] rules.

$$\tau_{LT} = \frac{4\psi_{LT}^2}{\kappa^2\alpha_{LT}^2 M_{y,Ed}/M_{y,pl}\left[1+\sqrt{1-4\beta\psi_{LT}\frac{M_{y,Ed}/M_{y,pl}-1}{\kappa^2\alpha_{LT}^2 M_{y,Ed}/M_{y,pl}}}\right]^2} \quad but \quad \tau_{LT} \leq 1$$
$$where \quad \psi_{LT} = 1 + \overline{\lambda}_{LT,0}\kappa\alpha_{LT}\frac{M_{y,Ed}}{M_{y,pl}} - \frac{M_{y,Ed}}{M_{y,pl}} \tag{11}$$

The adequacy of a beam is assessed through the out-of-plane buckling load factor, $\alpha_{cr,op}$; a value of $\alpha_{cr,op}$ greater than or equal to unity indicates that the beam possesses sufficient capacity, as shown in eq. (12). The ultimate capacity of a beam can be determined by iterating the applied bending $M_{y,Ed}$ until reaching $\alpha_{cr,op} = 1.0$.

$$\alpha_{cr,op} = \frac{\tau_{LT} M_{cr}}{M_{y,Ed}} \geq 1.0 \quad but \quad \tau_{LT} M_{cr} \leq M_{y,pl} \tag{12}$$

3.2. Moment gradient effect

For the case of beams subjected to varying bending moment along the span, use of the stiffness reduction function derived for uniform bending may lead to overly conservative results as the extent of plasticity is less in comparison to that for uniform bending. Thus, to achieve accurate strength predictions, this reduced extent of plastification must be taken into consideration. This may be achieved by (i) incorporating moment gradient factors into the stiffness reduction function τ_{LT} derived for uniform bending, and assuming a constant stiffness reduction rate for the whole laterally unrestrained segment of a beam or (ii) applying different stiffness reduction rates to different portions along the beam considering the corresponding bending moments. Both approaches have favourable aspects and limitations, as the former is easier to apply, but the latter can be employed for beams with any moment gradient shape. In the following two subsections, both approaches are investigated utilising results of a large number of GMNIA simulations considering a wide range of moment gradient shapes.

3.2.1. Allowance for moment gradient through moment gradient factors $C_{m,LT}$

In this subsection, the incorporation of moment gradient factors $C_{m,LT}$ into the stiffness reduction function derived for uniform bending is proposed to consider the influence of moment gradient on the development of plasticity. The moment gradient factors are incorporated into τ_{LT} given in eq. (11) as shown in eq. (13) where $M_{y,Ed}$ is the maximum absolute value of the moment along the laterally unrestrained length of a beam. To accurately identify the location of the out-of-plane failure, this paper recommends the calculation of different $C_{m,LT}$ and τ_{LT} values for each laterally unrestrained segment of a beam.

$$\tau_{LT} = \frac{4\psi_{LT}^2}{\kappa^2\alpha_{LT}^2 C_{m,LT} M_{y,Ed}/M_{y,pl}\left[1+\sqrt{1-3.2\psi_{LT}\frac{C_{m,LT}M_{y,Ed}/M_{y,pl}-1}{\kappa^2\alpha_{LT}^2 C_{m,LT}M_{y,Ed}/M_{y,pl}}}\right]^2} \quad but \quad \tau_{LT} \leq 1$$
$$where \quad \psi_{LT} = 1 + 0.2\kappa\alpha_{LT}\frac{C_{m,LT}M_{y,Ed}}{M_{y,pl}} - \frac{C_{m,LT}M_{y,Ed}}{M_{y,pl}} \quad (13)$$

The moment gradient factors $C_{m,LT}$ were calibrated to the GMNIA results of a series of fork-end supported beams, considering 7 European HE and IPE cross-sections and 66 typical loading cases. The change of $C_{m,LT}$ values for the case of beams subjected to different linearly varying bending moment diagrams is illustrated in Fig. 6, indicating that $C_{m,LT}$ values can be represented accurately as a function of the ratio of the end moments μ. Note that the $C_{m,LT}$ values were determined calibrating the LTB buckling curves obtained through eq. (12) and eq. (13) to those obtained through GMNIA and that these values are referred to as $C_{m,LT}-$GMNIA in the figure. The proposed equation of $C_{m,LT}$ for linearly varying bending moment diagrams is also shown in Fig. 6 which is derived through least square fitting to the $C_{m,LT}-$GMNIA values. Following the same approach, expressions for $C_{m,LT}$ were derived for various bending moment gradient shapes. The proposed expressions for the moment gradient factors $C_{m,LT}$ are provided in Table 5, where M, which is the maximum span moment, is also shown. Note that the $C_{m,LT}$ factors were derived assuming that the maximum moment coincided with the mid-length of the beam, but may also be conservatively applied when this is not the case. For the case of a point load acting away from the mid-length of the beam, a more refined expression for $C_{m,LT}$ is provided in Table 5. For beams subjected to both distributed and point loads, $C_{m,LT}$ expressions derived for moment diagrams associated with distributed loading can be conservatively employed, though in cases where the distributed loading only results from the self-weight of a beam or is small, its influence may be considered to be insignificant and $C_{m,LT}$ expressions derived for point load cases may be used.

The accuracy of incorporating the derived $C_{m,LT}$ factors into τ_{LT} is investigated for the 66 loading cases shown in Table 6, and for 7 different European IPE and HE section shapes whose depth to width ratios are within the range $0.958 \leq h/b \leq 2.5$, as shown in Table 7. Note that N is the number of beams considered for each loading case and S_{av}, S_{cov}, S_{min} and S_{max} are the average, coefficient of variation, maximum and minimum values of the ratios of the strengths obtained through LBA with stiffness reduction (LBA-SR) to those obtained through GMNIA respectively. In total, the LTB strengths of 1935 beams determined through LBA with the stiffness reduction scheme proposed in this subsection, which is referred to as the LBA-SR $C_{m,LT}$ approach, were compared against those obtained through GMNIA simulations in Table 7. In the application of the LBA-SR $C_{m,LT}$ approach, the actual loading conditions on the beams are considered and $C_{m,LT}$ factors, obtained from Table 5 for each corresponding loading condition, are only used in the determination of τ_{LT} whereby the Young's E and shear G moduli are reduced. The LTB slendernesses $\overline{\lambda}_{LT}$ of the analysed beams were between 0.4 and 2.0, increasing in increments of 0.2. Note that the results of very long beams whose length to depth ratios are larger than 50, $L/h > 50$, and those of beams not influenced by instability effects i.e. failing due to the attainment of maximum cross-section resistance are not included in the table. The results presented in Table 7 indicate that the proposed LBA-SR $C_{m,LT}$ approach leads to accurate LTB strength predictions for a wide range of loading cases and section shapes.

For beams with lateral restraints, this paper recommends the determination of $C_{m,LT}$, $M_{y,Ed}$ and therefore τ_{LT} values separately for each laterally unrestrained segment, provided that the lateral restraints at the both ends of a segment restrain the compression flange. If a lateral restraint does not restrain the compression flange, it should be neglected and the segment between the corresponding adjacent lateral restraints supporting the compression flange should be taken into account. After reducing the Young's E and shear G moduli of the segments appropriately, all lateral restraints, regardless of their position, should be included in the LBA. The application of the LBA-SR $C_{m,LT}$ approach to a multi-span beam is illustrated in Fig. 7, where $M_{y,Ed}$ and $C_{m,LT}$ values are used in the determination of τ_{LT} through eq. (13) for each laterally unrestrained segment. In the figure, $C_{m,LT}$ values are determined from Table 5, considering corresponding bending moment diagram for each segment.

3.2.2. Allowance for moment gradient through tapering approach

This section investigates the accuracy of the division of a beam into portions along the length and application of stiffness reduction factors to each portion considering corresponding bending moment values. The application of this approach is illustrated in Fig. 8. As can be seen from the figure, this process transforms the original beam into a 'stepped' beam, where different stiffness reduction rates are applied along the beam length. Since the stiffness of a beam is reduced gradually, the approach may be referred to as a tapering approach and this definition will henceforth be adopted in this paper. It should be noted that a stiffness reduction factor for each portion is determined using the value of the bending moment at the middle, as indicated in Fig. 8.

To assess the accuracy of the described approximation, the LTB strengths of fork-end supported beams with an IPE 240 cross-section and subjected to different moment diagram shapes are determined through GMNIA and Linear Buckling Analyses with the tapering approach, which is referred to as LBA-SR herein. The results of LBA-SR and GMNIA are compared in Fig. 9. Note that beams subjected to only end moments were divided into 4 to 10 portions, while those subjected to more complex loading cases were divided into 40 portions in the calculations presented in this section. As can be seen from Fig. 9 (a), the results obtained through LBA-SR are in a very good agreement with those of GMNIA for beams subjected to varying end moments. However, the tapering approach significantly overestimates the strength when a beam is subjected to transverse loading, as shown in Fig. 9 (b)-(d). This overestimation is attributed to the second-order torsional moments induced by transverse loading as the beam deflects laterally, leading to additional plasticity. This additional plasticity is not taken into account by τ_{LT} which was originally derived for beams subjected to equal and opposite end moments in Section 3.1. It should be noted that this additional plasticity, which is implicitly taken into account by the $C_{m,LT}$ factors in the LBA-SR $C_{m,LT}$ approach, is insignificant when lateral restraints are provided to the compression flange at the points of transverse loading for beams of practical proportions. To account for this effect, this study recommends the increase of the rate of stiffness reduction by using a larger imperfection factor α_{LT} value in τ_{LT} given by eq. (11), which will be denoted $\alpha_{LT,F}$ herein, with the 'F' indicating transverse loading. The recommended value of the increased imperfection factor is $\alpha_{LT,F} = 1.4\alpha_{LT}$, which was obtained through calibration to the GMNIA results. Using $\alpha_{LT,F} = 1.4\alpha_{LT}$ in τ_{LT}, the LTB strengths determined through LBA-SR were compared against those obtained through GMNIA in Fig. 9 (b)-(c). As can be seen from the figures, this approach provides accurate strength predictions. Unsurprisingly, the proposal leads to conservative predictions for beams subjected to small transverse loading but large end moments, and for beams where additional plasticity resulting from transverse loading is not induced in the proximity of the most heavily loaded cross-section. The latter is illustrated in Fig. 9 (d), where additional plasticity is induced within the moment gradient region of the beam, but not around the mid-span which is the most heavily loaded region, and hence the rate of the stiffness reduction should be lower.

The conservative errors resulting from the above proposal can be reduced considering the bending moment induced by transverse loading in the determination of $\alpha_{LT,F}$. Instead of using a constant value of $\alpha_{LT,F} = 1.4\alpha_{LT}$, the expression given by eq. (14) may be employed to determine $\alpha_{LT,F}$, where $M_{y,Ed,trans}$ is the maximum absolute bending moment value induced by transverse loading and $M_{y,Ed,max}$ is the maximum absolute bending moment value along the beam length. When $M_{y,Ed,trans} \leq 0.1M_{y,Ed,max}$, it is proposed to take $\alpha_{LT,F} = \alpha_{LT}$; this will reduce calculation effort for common cases, such as when lateral restraints are provided to the compression flange at the locations of point loads and the bending moment arising from transverse loading is only due to the selfweight of the beam. Note that the refined proposal for the determination of $\alpha_{LT,F}$ made herein is limited to determinate beams.

$$\begin{aligned} \alpha_{LT,F} &= \alpha_{LT}\left(1 + 0.4\frac{M_{y,Ed,trans}}{M_{y,Ed,max}}\right) \leq 1.4\alpha_{LT} \\ but \quad \alpha_{LT,F} &= \alpha_{LT} \quad if \quad \frac{M_{y,Ed,trans}}{M_{y,Ed,max}} \leq 0.1 \end{aligned} \tag{14}$$

In Table 7, the LTB strengths of beams obtained through the proposed tapering approach (i.e LBA-SR tapering) are compared against those determined through GMNIA for the 66 loading cases shown in Table 6. Three cross-section shapes were considered: IPE 500, IPE 240 and HEB 360 representing cross-sections with low, moderate and high torsional stiffness respectively. Table 7 indicates that the proposed LBA-SR tapering approach leads to accurate strength predictions and that the use of eq. (14) for the determination of $\alpha_{LT,F}$ in lieu of of using a constant value of $\alpha_{LT,F} = 1.4\alpha_{LT}$ increases the accuracy for beams subjected to both end moments and transverse loading.

Since the presented tapering approach uses bending moment values at the middle of each portions to determine τ_{LT} values, the division of a beam into an insufficient number of portions leads to the overestimation of the strength. The larger the number of portions, the smaller the strength prediction. Close convergence is achieved after dividing a beam into a sufficient number of portions, which is dependent on the shape of the bending moment diagram. Generally, in this study, the division of a beam into 40 portions was found to be sufficient for all considered moment diagram shapes, though fewer portions will often suffice, particularly in instances of low to moderate moment gradients. The required number of portions for a particular moment gradient shape can be determined through a convergence study.

Finally, it should be noted that in the all cases shown in this and previous sections, transverse loading was applied to the shear centre. The influence of the height of transverse loading on the LTB strengths of beams was also investigated though. In line with existing steel design codes [10, 12], it is proposed that load height is considered in the described LBA-SR approach directly through the change in elastic buckling moments M_{cr}, which was found to provide accurate predictions for the considered moment diagram shapes, i.e. provided the load height is correctly represented in the LBA, no further action is required.

4. Application of the proposed stiffness reduction method to LTB assessment of beams

Since the proposed stiffness reduction method (LBA-SR) provides the same strength predictions as those obtained using the LTB equation given by eq. (6) in Section 3.1 for regular members under uniform bending and its application to beams subjected to moment gradients is addressed in Section 3.2, this section focuses on the application of the method to irregular and multi-span beams. The LTB formula given by eq. (6) is also employed using elastic buckling moments M_{cr} obtained through LBA and determining LTB slendernesses $\overline{\lambda}_{LT}$, which is the traditional way to account for the influence of irregularities, so as to compare the proposed LBA-SR approach with the traditional design approach. To compare these two different design philosophies on a consistent basis, eq. (6) is adopted in preference to the Eurocode 3 LTB equations, since it provides more accurate strength predictions - see Table 4.

4.1. Stepped beam

The use of additional plates in the most heavily loaded regions (considering second-order effects) of a steel beam may considerably increase its strength. In this subsection, the accuracy of the proposed stiffness reduction method is investigated for the design of beams strengthened with additional plates, which may be referred to as stepped beams. Additional plates were attached to the flanges in the central half of a beam subjected to uniform bending, increasing the second moment of area to two times that of the original beam $I_{y2} = 2I_{y1}$, while the plastic section modulus became equal to 1.44 times of that of the original beam $W_{pl,y2} = 1.44W_{pl,y1}$. Linear Buckling Analysis with stiffness reduction (LBA-SR) was applied by separately reducing the stiffnesses of the strengthened and original portions through τ_{LT} given by eq. (11) considering the increased and original plastic bending moment resistances. The comparison of the strength predictions obtained through LBA-SR with those of GMNIA is illustrated in Fig. 10 for different slendernesses, where $\overline{\lambda}_{LT}$ values were determined using the elastic buckling moments of the stepped beams. The results indicate that LBA-SR leads to very accurate capacity predictions. In addition to LBA-SR, the traditional design approach using the LTB buckling curves given by eq. (6) was also carried out, with M_{cr} determined from LBA of the stepped beam. Fig. 10 indicates that LBA-SR provides more accurate strength predictions than this approach owing to the consideration of the different rates of plastification within the original and strengthened portions of the stepped beam.

4.2. Beam with an intermediate elastic lateral restraint

Application of the proposed stiffness reduction method to two beams with elastic lateral restraints and LTB slendernesses $\overline{\lambda}_{LT} = 0.8$ and $\overline{\lambda}_{LT} = 1.6$ is investigated in this subsection. The beams were subjected to uniform bending and the elastic restraints were applied to the compression flange at mid-span. Varying the stiffness of the elastic lateral restraint, the strengths of the beams were determined through GMNIA, Linear Buckling Analysis with stiffness reduction (LBA-SR) and the LTB formula given by eq. (6). In the application of GMNIA, two shapes of geometrical imperfections were considered: one half-sine wave and two-half sine waves corresponding to the first and second buckling modes of the beam. The LTB strength predictions are provided in Fig. 11, where K_L is the elastic threshold restraint stiffness to force the beam to buckle in the second mode, which was obtained through the finite element models. It may be seen from the figure that the single half-sine wave imperfection is critical up to a specific threshold restraint stiffness $K_{L,inelastic}$ for both beams. For larger restraint stiffness, the two half-sine wave imperfection results in lower strengths. This specific stiffness value can be referred to as the inelastic threshold stiffness $K_{L,inelastic}$ forcing the inelastic buckling of the beam in the second mode. Since the development of plasticity within the beam increases the effectiveness of the intermediate elastic lateral restraint, the threshold stiffness forcing inelastic buckling in the second mode $K_{L,inelastic}$ is lower than that required for elastic buckling K_L, i.e. $K_{L,inelastic} \leq K_L$. Fig. 11 shows that LBA-SR captures this increased effectiveness, providing strength predictions in close agreement with those obtained through GMNIA. It is also noteworthy that while GMNIA requires the application of two different shapes of geometrical imperfections, LBA-SR directly captures the transition between the first and second inelastic buckling modes after exceeding the inelastic threshold stiffness $K_{L,inelastic}$. The ratio of $K_{L,inelastic}/K_L$ is dependent on the extent of plasticity undergone by the beams: the greater the extent of plasticity, the smaller the ratio. This can be seen by comparing Fig. 11 (a) and (b). Since the development of plasticity within the beams was not considered, the use of the calibrated LTB formula given in eq. (6) with the elastic buckling moments obtained through LBA provides less accurate and overly-conservative results for the beam with $\overline{\lambda}_{LT} = 0.8$, which experiences a greater extent of plasticity in comparison to the more slender beam with $\overline{\lambda}_{LT} = 1.6$.

4.3. Braced beam

In this subsection, application of the stiffness reduction method to the design of a braced beam is investigated. The geometrical properties and loading conditions of the braced beam of IPE 240 cross-section are displayed in Fig. 12. In the implementation of LBA-SR, both the moment gradient factor $C_{m,LT}$ approach i.e. LBA-SR $C_{m,LT}$ approach, described in Section 3.2.1, and the tapering approach i.e. LBA-SR tapering approach, described in Section 3.2.2, were employed. Considering the shape of the bending moment diagram, different levels of stiffness reduction were applied to the external and internal laterally unrestrained segments of the beam in the implementation of the LBA-SR $C_{m,LT}$ approach, using the $C_{m,LT}$ values given in Table 5. In the application of the LBA-SR tapering approach, the imperfection factor was taken as $\alpha_{LT,F} = \alpha_{LT}$ as lateral and torsional restraints are provided at the points where the transverse loads are applied. GMNIA of the beam was performed using its lowest buckling mode as the initial imperfection shape, with a magnitude of $L/1000$. The calibrated LTB formula given by eq. (6) was employed using elastic critical moments obtained through LBA to make capacity predictions. Since the central segment under uniform bending is critical, the LTB formula calibrated for beams under uniform bending can be used for this beam. The LTB formula was also applied assuming each laterally unrestrained segment to be an individual simply supported beam and using the critical segment to govern the ultimate strength of the whole beam. Note that this design approach, which is popular due to its simplicity, was first recommended by Salvadori [32] and is referred to as the Salvadori lower bound assumption in the literature [4, 33] as it disregards the restraining effect provided by adjacent segments. The comparison of the results for different slenderness values are provided in Fig. 12, where $\overline{\lambda}_{LT}$ is determined considering the elastic critical moment of the whole beam. It is clearly seen from the figure that the agreement between the strength predictions obtained through both the LBA-SR $C_{m,LT}$ and LBA-SR tapering approaches, and those determined through GMNIA is very good. Moreover, the LBA-SR approach leads to more accurate strength predictions in comparison to use of the LTB formula with M_{cr} from LBA since unlike this method, the LBA-SR approach considers the development of different extents of plasticity within the different segments of the beam. For this beam, the central unrestrained length undergoes a high degree of plasticity and the relative support afforded by the adjacent segments, which remain largely elastic, effectively increases, thus increasing the ultimate strength of the beam. Since both the restraining effect provided by adjacent segments and the development different levels of plasticity within the segments are not considered, use of the LTB equation with the Salvadori lower bound assumption leads to very overly conservative results, as seen from Fig. 12.

4.4. Continuous beam

This subsection addresses the application of the stiffness reduction method to a three-span continuous beam with an IPE 240 cross-section and subjected to a uniformly distributed load applied to the top flange. The geometrical properties and loading conditions of the beam are illustrated in Fig. 13. The LTB strengths of the beam were determined through GMNIA, the LBA-SR $C_{m,LT}$ approach and the LBA-SR tapering approach. Additionally, the Eurocode 3 specific case LTB equation was employed to predict the LTB strengths using elastic critical moments from LBA and through the Salvadori lower bound assumption. Unlike the other cases addressed in the previous subsections, the LTB equation given in eq. (6) is not used herein as it does not consider the influence of moment gradient on plasticity (when used outside of the stiffness reduction framework), thus leading to less accurate results in comparison to the Eurocode 3 specific case LTB equation. GMNIA of the beams were performed adopting the lowest buckling modes as the imperfection shapes, with a magnitude of L/1000. In the application of LBA-SR, stiffness reduction is applied on the basis of the elastic bending moment diagram. Using Table 5, different $C_{m,LT}$ values were determined for each span, within which constant stiffness reductions were applied using eq. (13) in the implementation of the LBA-SR $C_{m,LT}$ approach. The comparison between the strength predictions obtained through GMNIA, the LBA-SR $C_{m,LT}$ and LBA-SR tapering approaches, and the Eurocode 3 specific case LTB equation is shown in Fig. 13, where $\overline{\lambda}_{LT}$ is determined considering the elastic critical moment of the continuous beam. Note that the maximum strengths are limited to $M_{y,pl}$ indicating the attainment of the plastic moment capacity at the most heavily loaded section in the figure and that the strengths obtained through GMNIA exceeded these values for stocky beams due to moment redistribution and strain hardening. Fig. 13 shows that the correlation between the strength predictions made through both the LBA-SR $C_{m,LT}$ and LBA-SR tapering approaches and those obtained through GMNIA is quite good. Both the LBA-SR $C_{m,LT}$ and LBA-SR tapering approaches generally lead to more accurate results in comparison to those obtained through the Eurocode 3 specific case formula. It is of interest to note that unlike the previous example, the differences between the LTB strengths determined using elastic critical moments from LBA and assuming the Salvadori lower bound is not substantially different as the outer segments are critical and subjected to double curvature bending for this case.

5. Conclusions

The use of stiffness reduction for the lateral-torsional buckling assessment of steel members has been investigated in this study. Shell finite element models of steel beams were developed and validated against experimental results from the literature. An LTB assessment formula was proposed and calibrated to the GMNIA results of around 300 beams considering 30 different European section shapes. The proposed formula was then utilised to derive an accurate and compact stiffness reduction function. The developed stiffness reduction function was applied by reducing both the Young's modulus E and shear modulus G and performing LBA to determine the LTB strengths of regular, irregular, single span and multi-span beams. For the irregular and multi-span beams, more accurate results were achieved in comparison to those obtained through traditional methods. The influence of the bending moment gradient on the development of plasticity was thoroughly investigated. To consider this influence, this paper proposed a practical approach based on the incorporation of moment gradient factors into the stiffness reduction function originally derived for uniform bending. GMNIA simulations of 1935 beams were performed considering 66 different loading cases to calibrate moment gradient factors for a series of typical shapes of bending moment diagram, and the accuracy of the proposed approach was verified utilising these results. In addition to this method, a tapering approach, based on the division of a beam into portions along the length and reduction of their stiffnesses considering the corresponding moments, was also investigated. Proposals that significantly enhance the accuracy of the tapering approach for members subjected to transverse loading between lateral restraints were made.

The proposed stiffness reduction method, which can readily be applied through any software providing accurate elastic critical moments through LBA, obviates the need for using LTB assessment equations and considers the influence of the development of plasticity on the response of steel beams, so offering a realistic and practical means of design. The presented study is part of a wider research effort aiming to develop a design framework based on the separation of in-plane and out-of-plane analyses of steel members or frames subjected to in-plane loading. Thus, the stiffness reduction method presented in this study may be used in conjunction with that proposed for in-plane design in Kucukler et al. [20]. Future research will be directed towards the extension of the method to the flexural-torsional buckling assessment of steel beam-columns and frames.

References

[1] ECCS. Manual on stability of steel structures. Technical Committee 8 of European Convention for Constructional Steelwork (ECCS), No. 22; 1976.

[2] Galambos, T.V., Ravindra, M.. Load and resistance factor design criteria for steel beams. Structural Division, Civil and Environmental Engineering Department, Washington University; 1974.

[3] Yura, J.A., Ravindra, M.K., Galambos, T.V.. The bending resistance of steel beams. ASCE, Journal of the Structural Division 1978;104(9):1355–1370.

[4] Nethercot, D.A., Trahair, N.S.. Inelastic lateral buckling of determinate beams. ASCE, Journal of the Structural Division 1976;102(4):701–717.

[5] Ziemian, R.D.. Guide to stability design criteria for metal structures. John Wiley & Sons; 2010.

[6] Neal, B.G.. The lateral instability of yielded mild steel beams of rectangular cross-section. Proceedings of Royal Society 1950;242:197–242.

[7] Horne, M.R.. Critical loading conditions in engineering structures. Ph.D. thesis; University of Cambridge.; 1950.

[8] Wittrick, W.H.. Lateral instability of rectangular beams of strain hardening material under uniform bending. Journal of Aeronautical Science 1952;19(12).

[9] Trahair, N.S., Kitipornchai, S.. Buckling of inelastic i-beams under uniform moment. ASCE, Journal of the Structural Division 1972;98(11):2551–2566.

[10] EN 1993-1-1, Eurocode 3 Design of steel structures-Part 1-1: General rules and rules for buildings. European Committee for Standardization (CEN), Brussels; 2005.

[11] AISC-360-10, Specifications for structural steel buildings. Chicago; 2010.

[12] Standards Australia, AS 4100 steel structures. Australian Building Codes Board, Sydney; 1998.

[13] Wongkaew, K.. Practical advanced analysis for design of laterally unrestrained steel planar frames under in-plane loads. Ph.D. thesis; Purdue University; 2000.

[14] Wongkaew, K., Chen, W.F.. Consideration of out-of-plane buckling in advanced analysis for planar steel frame design. Journal of Constructional Steel Research 2002;58(5):943–965.

[15] Trahair, N.S., Chan, S.L.. Out-of-plane advanced analysis of steel structures. Engineering Structures 2003;25(13):1627–1637.

[16] Trahair, N.S., Hancock, G.J.. Steel member strength by inelastic lateral buckling. ASCE, Journal of Structural Engineering 2003;130(1):64–69.
[17] AISC-LRFD, Load and resistance factor design specification for structural steel buildings. AISC, Chicago; 1993.
[18] Trahair, N.S.. Steel cantilever strength by inelastic lateral buckling. Journal of Constructional Steel Research 2010;66(8):993–999.
[19] Trahair, N.S.. Inelastic buckling design of monosymmetric I-beams. Engineering Structures 2012;34:564–571.
[20] Kucukler, M., Gardner, L., Macorini, L.. A stiffness reduction method for the in-plane design of structural steel elements. Engineering Structures 2014;73:72–84.
[21] Abaqus v.6.10 Reference Manual. Simulia, Dassault Systemes; 2010.
[22] ECCS, Ultimate limit state calculation of sway frames with rigid joints. Tech. Rep.; No. 33, Technical Committee 8 (TC 8) of European Convention for Constructional Steelwork (ECCS); 1984.
[23] Crisfield, M.A.. A fast incremental/iterative solution procedure that handles snap-through. Computers & Structures 1981;13(1):55–62.
[24] Ramm, E.. Strategies for tracing the non-linear response near the limit points. In: Nonlinear Finite Element Analysis in Structural Mechanics. Springer Berlin Heidelberg; 1981, p. 63–89.
[25] AISC Code of Standard Practice for Steel Buildings and Bridges. American Institute of Steel Construction; 2010.
[26] Dux, P.F., Kitipornchai, S.. Inelastic beam buckling experiments. Journal of Constructional Steel Research 1983;3(1):3–9.
[27] Rebelo, C., Lopes, N., Simões da Silva, L., Nethercot, D.A., Vila Real, P.. Statistical evaluation of the lateral-torsional buckling resistance of steel I-beams, Part I: Variability of the Eurocode 3 resistance model. Journal of Constructional Steel Research 2009;65(4):818–831.
[28] Stangenberg, H.. Zum bauteilnachweis offener, stabilitätsgefährdeter stahlbauprofile unter einbeziehung seitlicher beanspruchungen und torsion. Ph.D. thesis; RWTH Aachen; 2007.
[29] Taras, A., Greiner, R.. New design curves for lateral–torsional buckling-Proposal based on a consistent derivation. Journal of Constructional Steel Research 2010;66(5):648–663.
[30] Greiner, R., Salzgeber, G., Ofner, R.. New lateral-torsional buckling curves χ_{LT} - Numerical simulations and design formulae. ECCS TC8 Report No. TC-8-2000-014; 2000.
[31] Byfield, M.P., Nethercot, D.A.. An analysis of the true bending strength of steel beams. Proceedings of the ICE-Structures and Buildings 1998;128(2):188–197.
[32] Salvadori, M.. Lateral buckling of beams of rectangular cross section under bending and shear. In: Proceedings, 1st US Congress of Applied Mechanics. 1951,.
[33] Dux, P.F., Kitipomchai, S.. Buckling approximations for inelastic beams. ASCE, Journal of the Structural Engineering 1984;110(3):559–574.

Figures captions

Figure 1 : Material model used in finite element simulations

Figure 2 : Residual stress patterns applied to finite element models (+ve = tension, -ve = compression)

Figure 3 : Calibration of the generalised imperfection factor η_{LT} using the GMNIA results of fork-end supported beams subjected to uniform major axis bending

Figure 4 : Derivation of a stiffness reduction function τ_{LT} for lateral-torsional buckling

Figure 5 : Stiffness reduction for different cross-section shapes

Figure 6 : Calibration of moment gradient factors $C_{m,LT}$ for linearly varying bending moment diagrams

Figure 7 : Application of LBA-SR $C_{m,LT}$ approach to a multi-span beam

Figure 8 : Application of different stiffness reduction rates along the beam length - Tapering approach

Figure 9 : Comparison of LTB strengths determined through Linear Buckling Analysis with stiffness reduction through the tapering approach (LBA - SR) against those of GMNIA for different bending moment diagrams

Figure 10 : Comparison of the LTB strengths determined through LBA-SR (i.e. stiffness reduction method) with those from GMNIA and the LTB formula proposed in this study for a stepped beam

Figure 11 : Comparison of LTB strengths determined through LBA-SR with those from GMNIA and the LTB formula for beams with elastic lateral restraints - δ_0 and θ_0 are initial out-of-straightness and twist

Figure 12 : Comparison of the LTB strengths determined through LBA-SR (i.e. stiffness reduction method) with those from GMNIA and the LTB formula proposed in this study for a braced beam

Figure 13 : Comparison of the LTB strengths determined through LBA-SR (i.e. stiffness reduction method) with those from GMNIA and the Eurocode 3 specific case LTB formula for a continuous beam

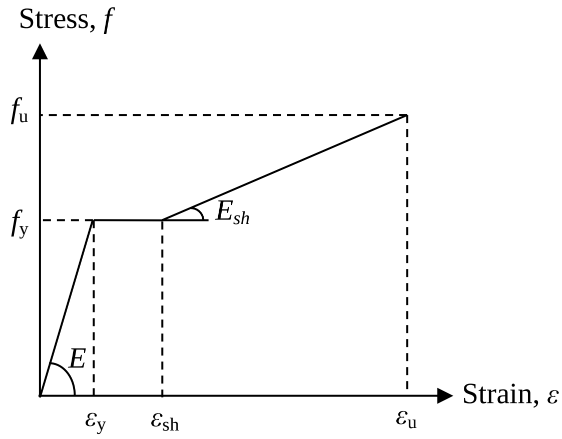

Figure 1: Material model used in finite element simulations

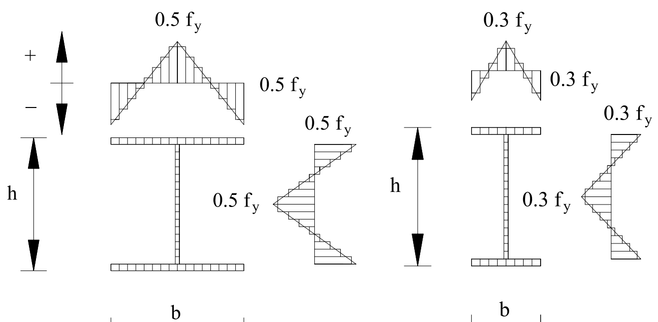

(a) h / b $\leq$ 1.2
(b) h / b $>$ 1.2

Figure 2: Residual stress patterns applied to finite element models (+ve = tension, -ve = compression)

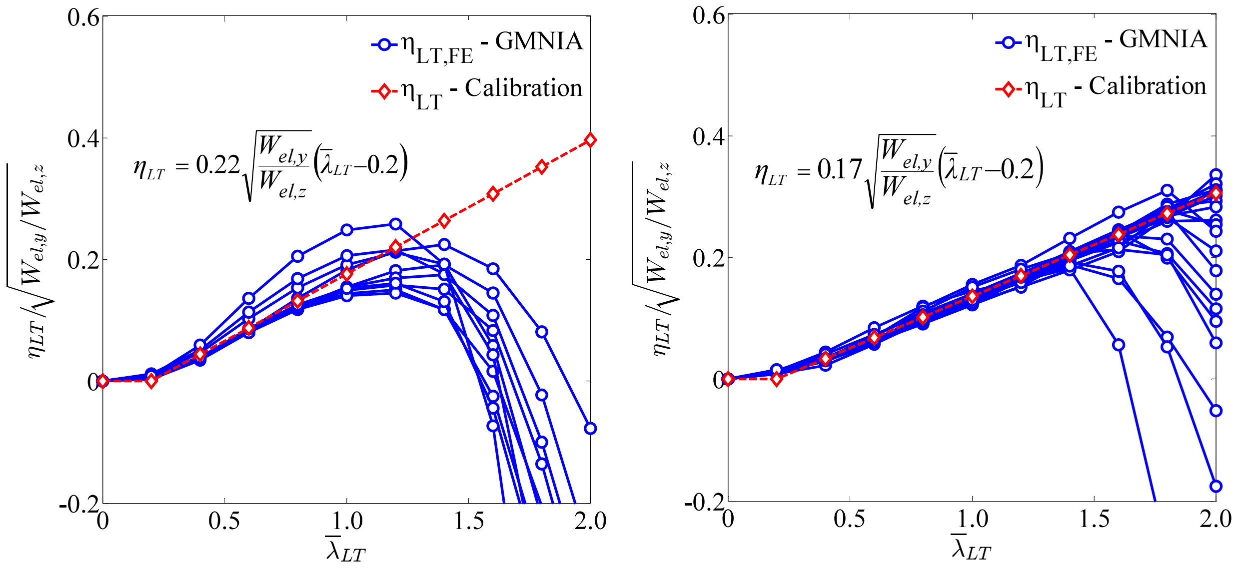

(a) $h/b \leq 1.2$

(b) $h/b > 1.2$

Figure 3: Calibration of the generalised imperfection factor η_{LT} using the GMNIA results of fork-end supported beams subjected to uniform major axis bending

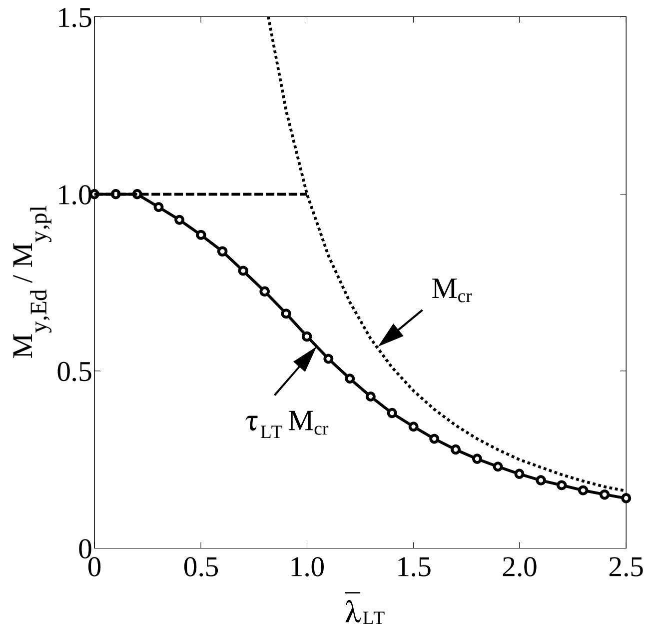

Figure 4: Derivation of a stiffness reduction function τ_{LT} for lateral-torsional buckling

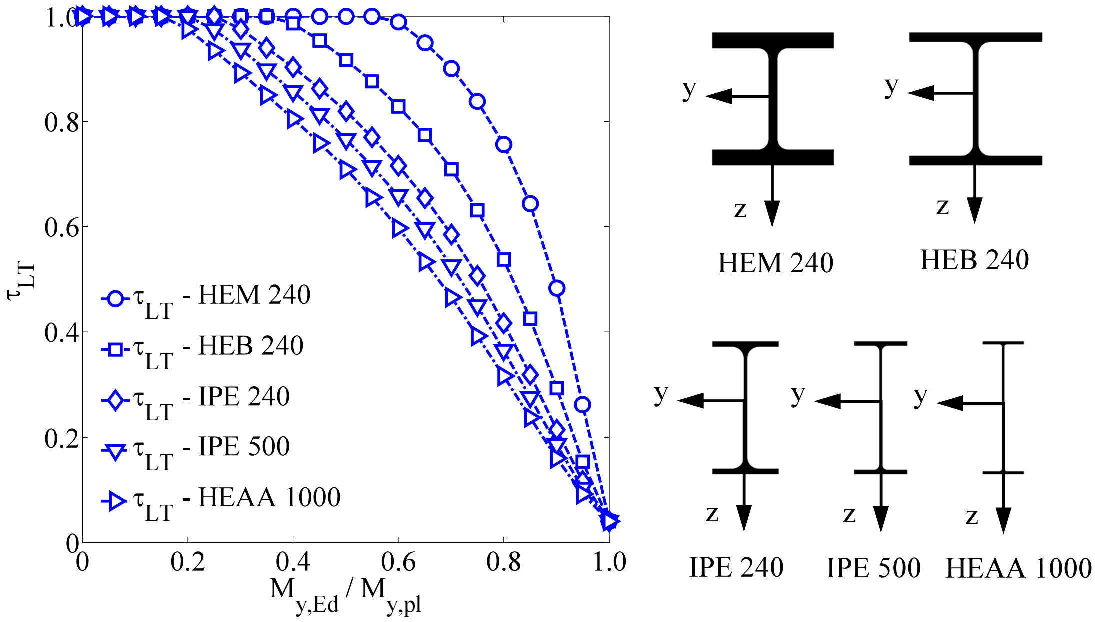

Figure 5: Stiffness reduction for different cross-section shapes

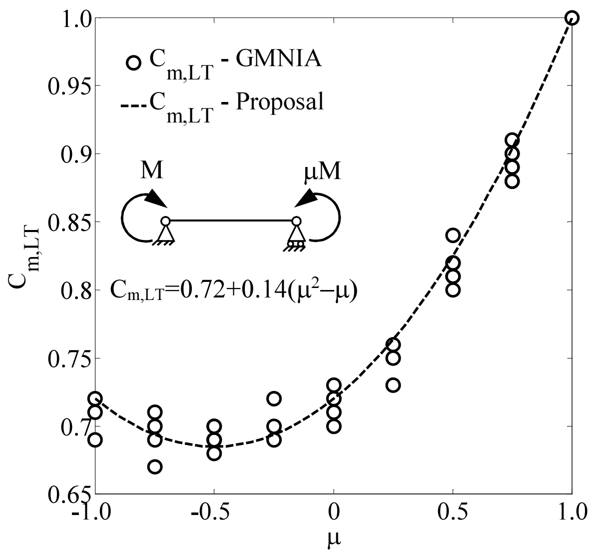

Figure 6: Calibration of moment gradient factors $C_{m,LT}$ for linearly varying bending moment diagrams

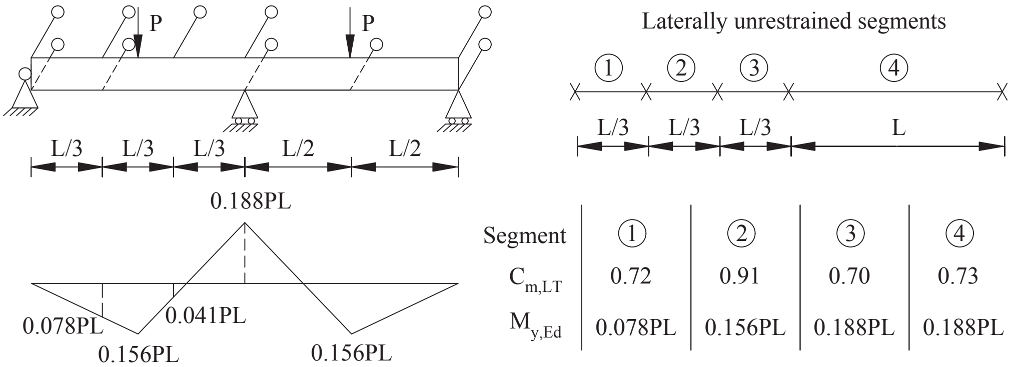

Segment	1	2	3	4
$C_{m,LT}$	0.72	0.91	0.70	0.73
$M_{y,Ed}$	0.078PL	0.156PL	0.188PL	0.188PL

Figure 7: Application of LBA-SR $C_{m,LT}$ approach to a multi-span beam

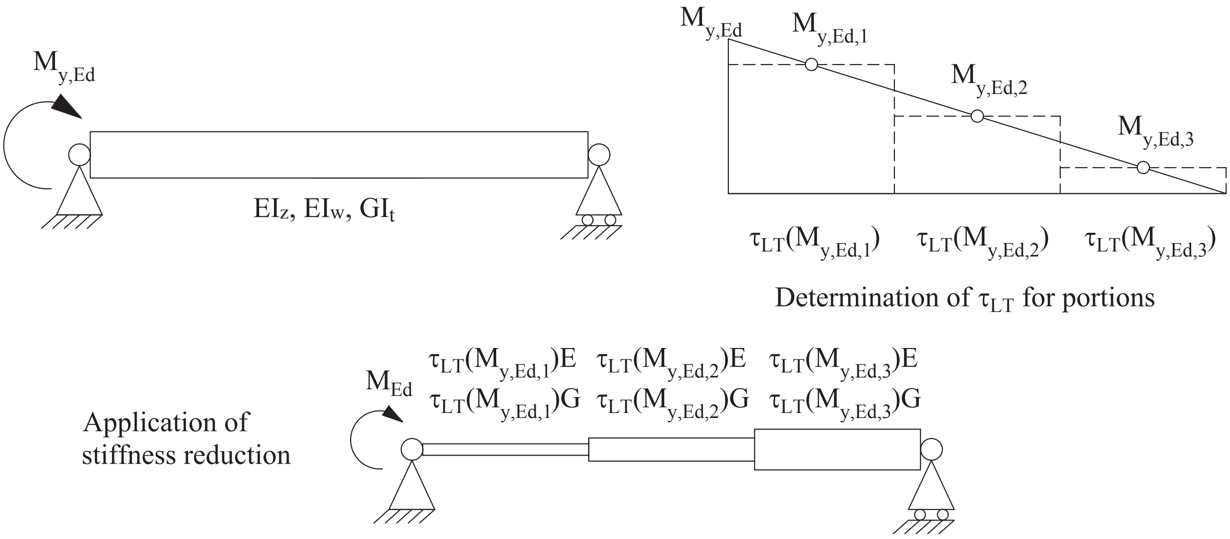

Figure 8: Application of different stiffness reduction rates along the beam length - Tapering approach

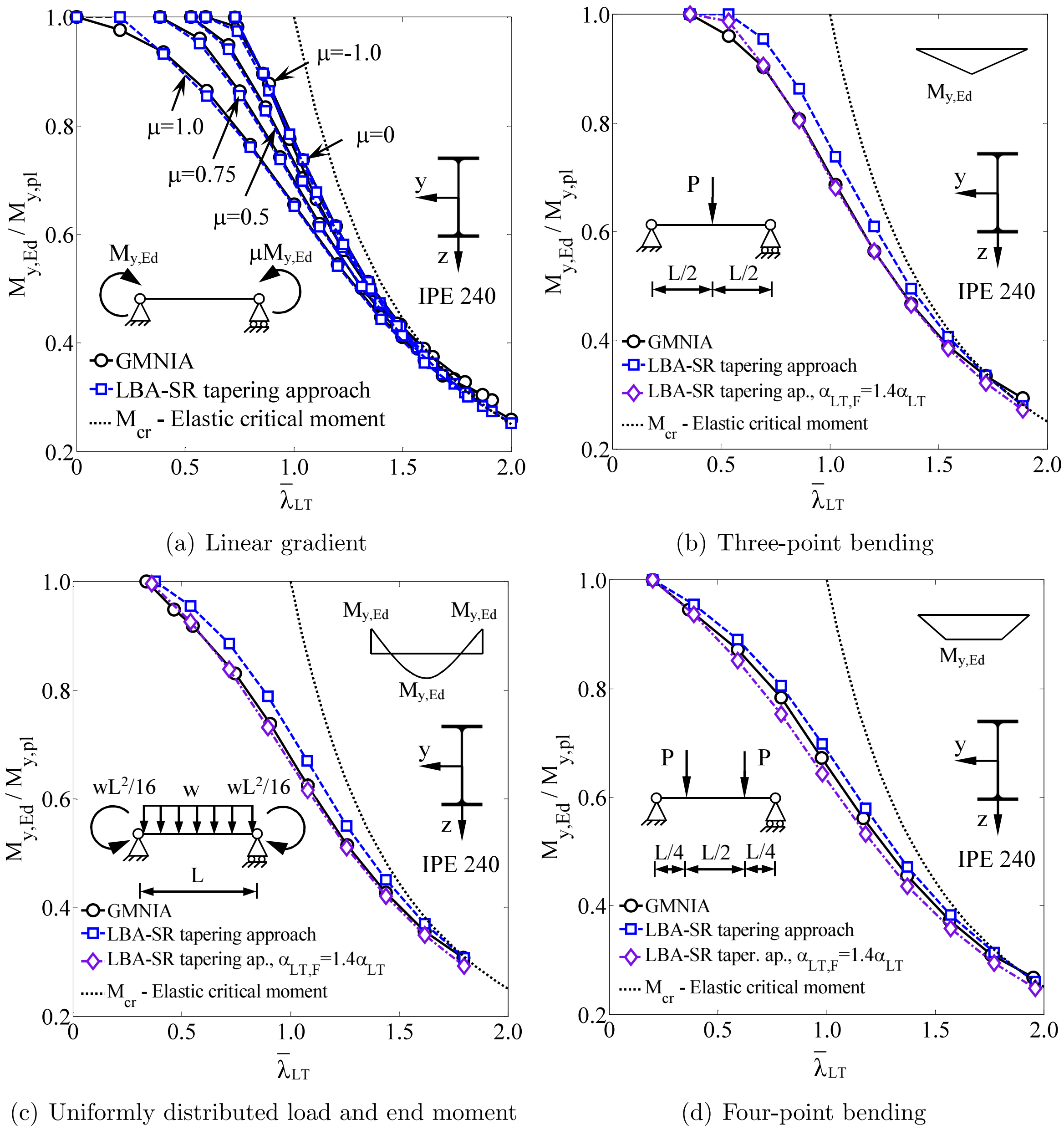

Figure 9: Comparison of LTB strengths determined through Linear Buckling Analysis with stiffness reduction through the tapering approach (LBA - SR) against those of GMNIA for different bending moment diagrams

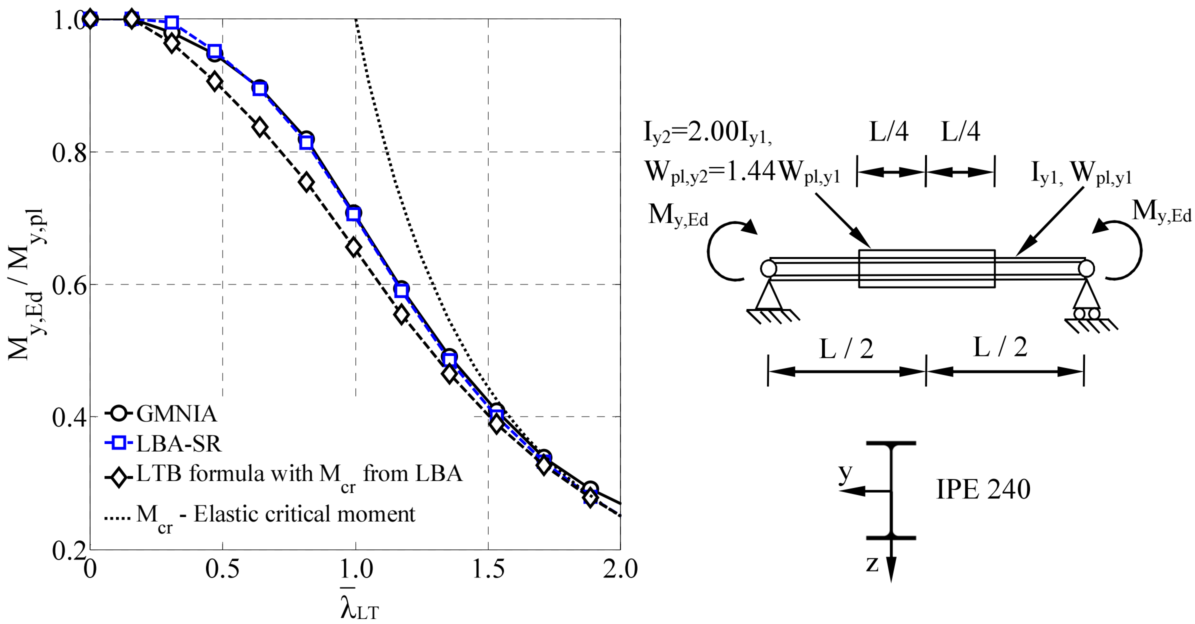

Figure 10: Comparison of the LTB strengths determined through LBA-SR (i.e. stiffness reduction method) with those from GMNIA and the LTB formula proposed in this study for a stepped beam

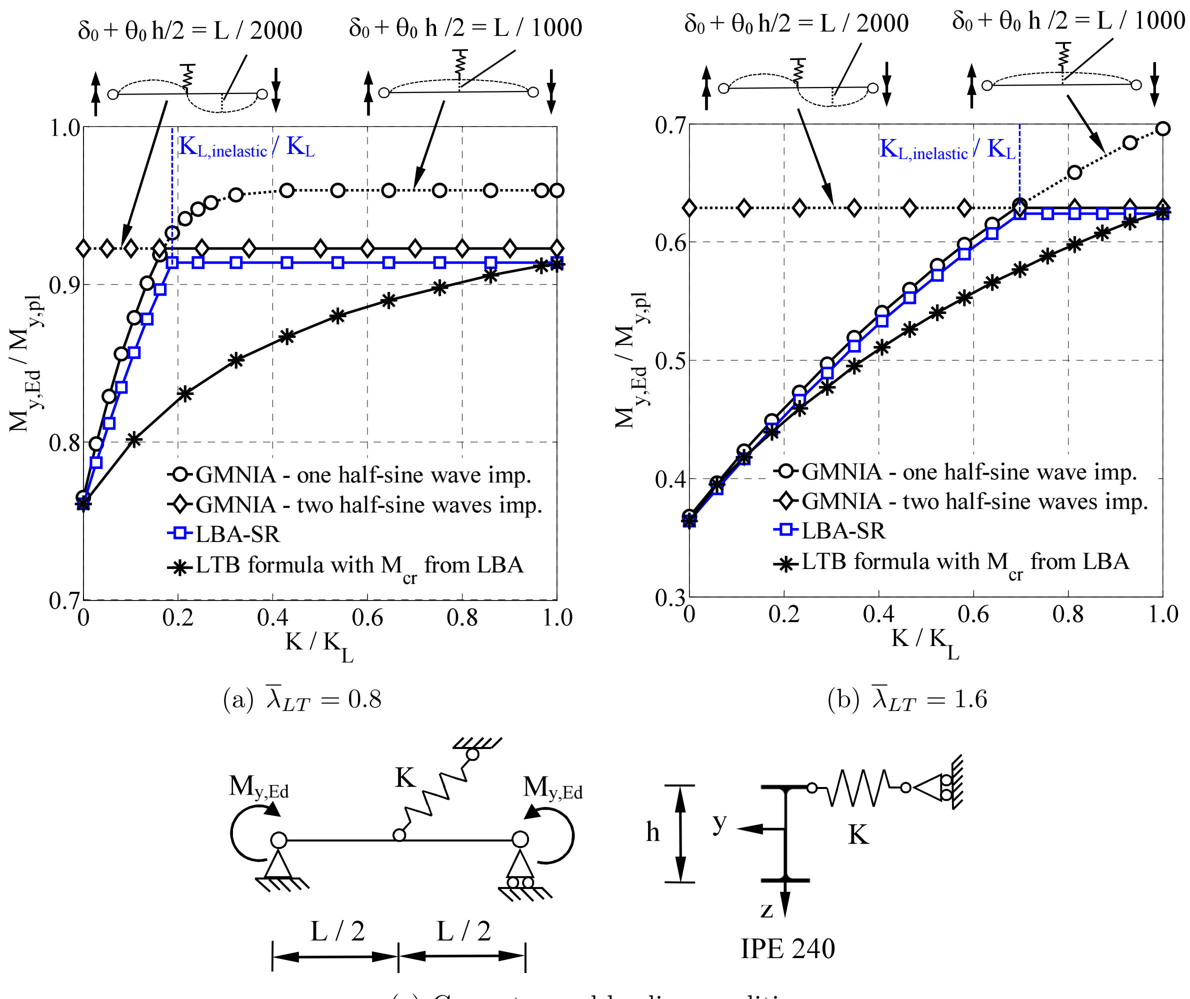

(c) Geometry and loading conditions

Figure 11: Comparison of LTB strengths determined through LBA-SR with those from GMNIA and the LTB formula for beams with elastic lateral restraints - δ_0 and θ_0 are initial out-of-straightness and twist

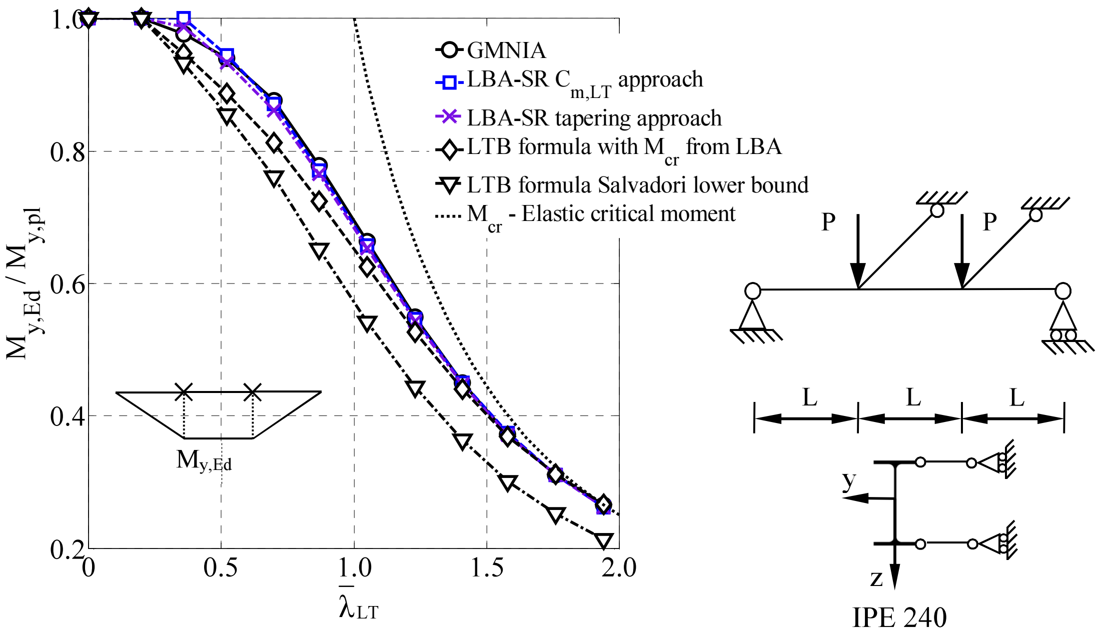

Figure 12: Comparison of the LTB strengths determined through LBA-SR (i.e. stiffness reduction method) with those from GMNIA and the LTB formula proposed in this study for a braced beam

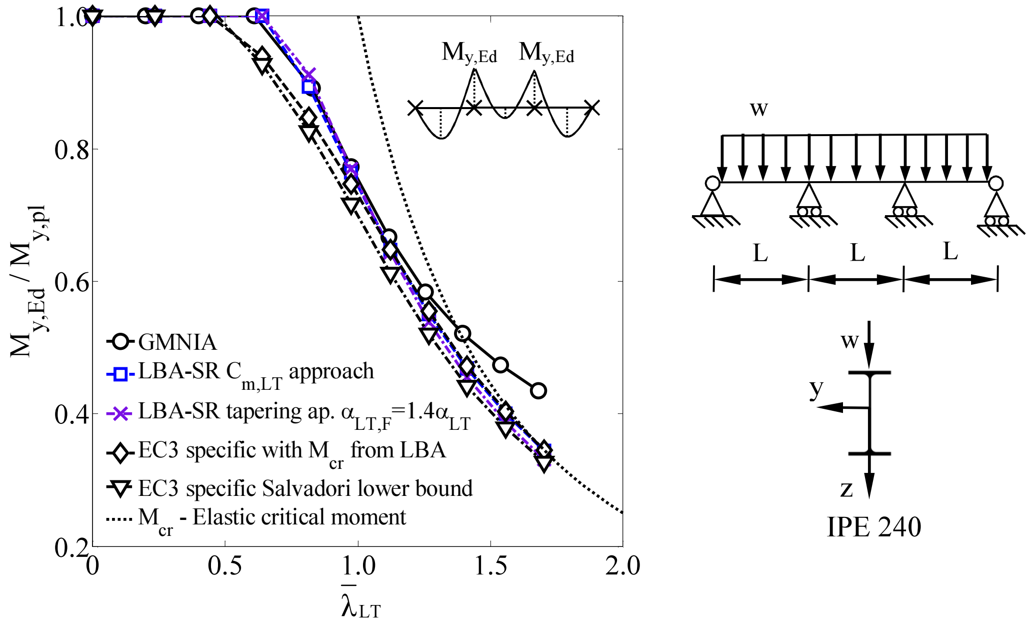

Figure 13: Comparison of the LTB strengths determined through LBA-SR (i.e. stiffness reduction method) with those from GMNIA and the Eurocode 3 specific case LTB formula for a continuous beam

Tables captions

Table 1 : Comparison of the strength predictions made by the finite element models with the experimental results reported by Dux and Kitipornchai [26]

Table 2 : Range of the European I cross-section dimensions used for calibration of the formulae proposed in this study

Table 3 : Values of α_{LT}, β, $\overline{\lambda}_{LT,0}$ and κ proposed in this study and those given in Eurocode 3-1-1 (2005)

Table 4 : Comparison of the LTB strengths obtained through the proposed LTB formula against those obtained through GMNIA and the Eurocode 3 general and specific case formulae

Table 5 : Calibrated moment gradient factors $C_{m,LT}$ for typical bending moment diagram shapes - μ, α and β are positive if they have the same sign with M

Table 6 : Considered load cases for the assessment of the proposed stiffness reduction approaches - Negative values of μ,α indicate that applied moment is in the opposite direction to that shown

Table 7 : Accuracy of the proposed approaches for the consideration of moment gradient effects

Table 1: Comparison of the strength predictions made by the finite element models with the experimental results reported by Dux and Kitipornchai [26]

Loading conditions	L (m)	$\overline{\lambda}_{LT}$	$M_{ult,exp}/M_{y,pl}$	$M_{ult,FE}/M_{y,pl}$	$M_{ult,FE}/M_{ult,exp}$
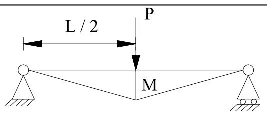	11	0.96	0.917	0.882	0.96
	9	0.83	0.990	0.983	0.99
	8	0.76	1.010	1.000	0.99
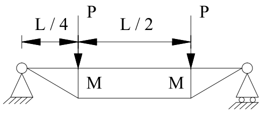	6	0.59	0.958	0.905	0.94
	5	0.50	0.949	0.938	0.99
	7	0.68	0.883	0.834	0.94
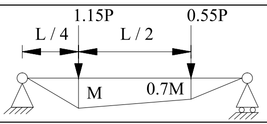	7	0.62	0.996	0.941	0.94
	8	0.70	0.960	0.949	0.99
	9	0.77	0.925	0.933	1.01
				Mean	0.97
				COV	0.026

Table 2: Range of the European I cross-section dimensions used for calibration of the formulae proposed in this study

	$h/b \leq 1.2$ - 10 sections		$h/b > 1.2$ - 20 sections	
	Max	Min	Max	Min
h/b	1.2	0.91	3.34	1.22
b/t_f	25	5.3	23.08	7.55
h/t_w	37.67	10	60.92	17.95

Table 3: Values of α_{LT}, β, $\overline{\lambda}_{LT,0}$ and κ proposed in this study and those given in Eurocode 3-1-1 (2005)

	This study		Eurocode 3 specific		Eurocode 3 general	
Aspect ratio	$h/b \leq 1.2$	$h/b > 1.2$	$h/b \leq 2.0$	$h/b > 2.0$	$h/b \leq 2.0$	$h/b > 2.0$
α_{LT}	$0.22\sqrt{\frac{W_{el,y}}{W_{el,z}}}$	$0.17\sqrt{\frac{W_{el,y}}{W_{el,z}}}$	0.34	0.49	0.21	0.34
β	0.80	0.80	0.75	0.75	1.00	1.00
$\overline{\lambda}_{LT,0}$	0.20	0.20	0.40	0.40	0.20	0.20
κ	see - eq. (3)		1.00	1.00	1.00	1.00

Table 4: Comparison of the LTB strengths obtained through the proposed LTB formula against those obtained through GMNIA and the Eurocode 3 general and specific case formulae

	Aspect ratio	N	S_{av}	S_{COV}	S_{max}	S_{min}
This study - eq. (6)			1.00	0.013	1.04	0.97
Eurocode 3 - General case	h / b > 1.2	151	0.95	0.061	1.08	0.84
Eurocode 3 - Specific case			1.03	0.034	1.11	0.93
This study - eq. (6)			0.99	0.019	1.03	0.94
Eurocode 3 - General case	h / b $\leq$ 1.2	47	0.99	0.035	1.06	0.90
Eurocode 3 - Specific case			1.02	0.030	1.09	0.96

Table 5: Calibrated moment gradient factors $C_{m,LT}$ for typical bending moment diagram shapes - μ, α and β are positive if they have the same sign with M

Shape of bending moment diagram	Range	$C_{m,LT}$
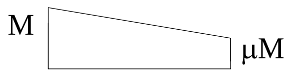	$-1 \leq \mu \leq 1$	$0.72 + 0.14(\mu^2 + \mu)$
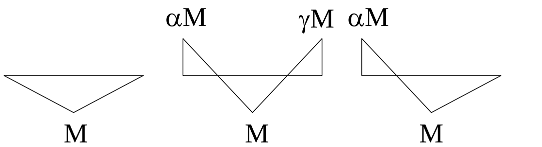	$-1 \leq \alpha \leq 0$ & $-1 \leq \gamma \leq 0$	0.88
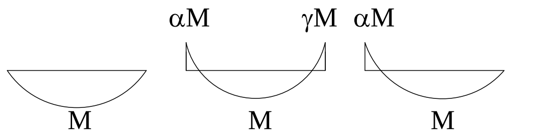	$-1 \leq \alpha \leq 0$ & $-1 \leq \gamma \leq 0$	0.95
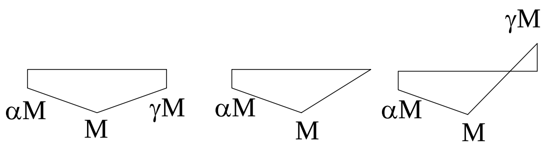	$0 \leq \alpha \leq 1$ & $\gamma \leq \alpha$	$0.88 + 0.12\alpha^2$
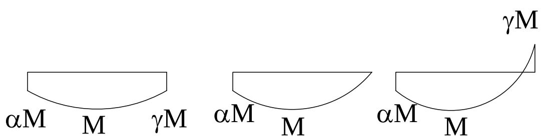	$0 \leq \alpha \leq 1$ & $\gamma \leq \alpha$	$0.95 + 0.05\alpha^2$
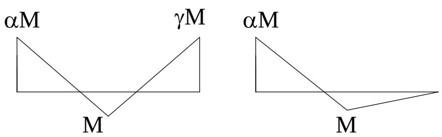	$\alpha \leq -1$ & $\gamma \leq 0$	$0.88 - 0.4(-\alpha - 1)^{0.6} \geq 0.60$
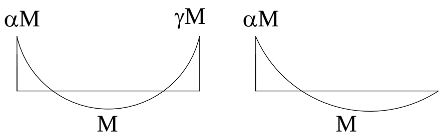	$\alpha \leq -1$ & $\gamma \leq 0$	$0.95 - 0.4(-\alpha - 1)^{0.6} \geq 0.55$
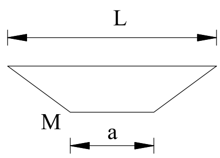	$0 \leq a \leq L$	$0.88 + 0.18(a/L)^{0.5} \leq 1.0$
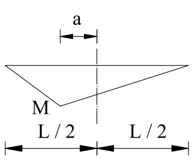	$0 \leq a \leq L/2$	$0.88 - 0.16(2a/L)^3$

Table 6: Considered load cases for the assessment of the proposed stiffness reduction approaches - Negative values of μ,α indicate that applied moment is in the opposite direction to that shown

Load case	Variable	Load case	Variable
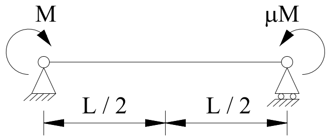	μ=-1.0,-0.75,-0.5, -0.25,0,0.25,0.5,0.75	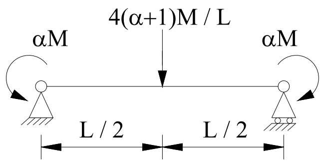	α=-0.75,-0.5, -0.25,0,0.5,1.0 1.25,1.5,1.75,2.0
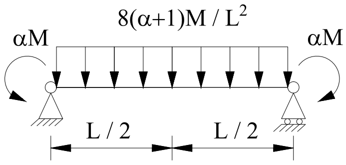	α=-0.75,-0.5, -0.25,0,0.5,1.0 1.25,1.5,1.75,2.0	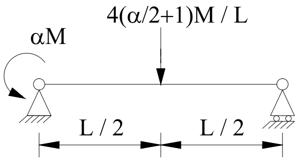	α=-0.75,-0.5, -0.25,0,0.5,1.0 1.25,1.5,1.75,2.0
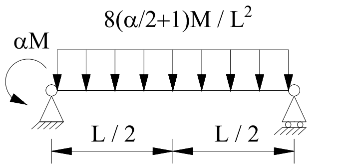	α=-0.75,-0.5, -0.25,0,0.5,1.0 1.25,1.5,1.75,2.0	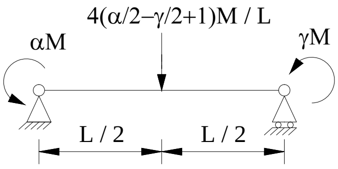	α=0.5,1.0 γ=0.25,0.5,0.75
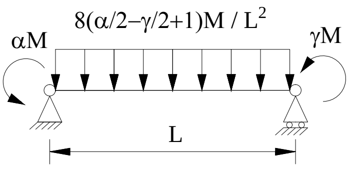	α=0.5,1.0 γ=0.25,0.5,0.75	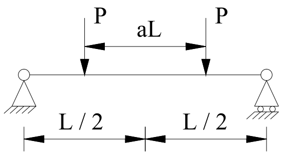	a=0.25,0.5,0.75
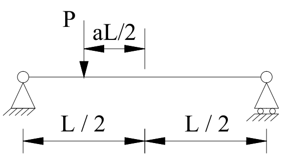	a=0.25,0.5,0.75		

Table 7: Accuracy of the proposed approaches for the consideration of moment gradient effects

Load case	Analysis approach	N	S_{av}	S_{cov}	S_{max}	S_{min}
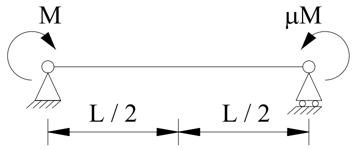	LBA-SR $C_{m,LT}$ approach	216	1.00	0.013	1.04	0.96
	LBA-SR tapering $\alpha_{LT,F} = \alpha_{LT}$	119	1.00	0.012	1.02	0.96
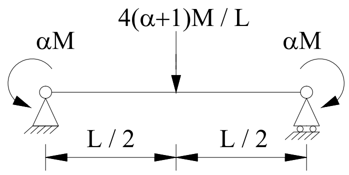	LBA-SR $C_{m,LT}$ approach	320	1.00	0.016	1.06	0.96
	LBA-SR tapering $\alpha_{LT,F} = 1.4\alpha_{LT}$	155	0.98	0.034	1.05	0.90
	LBA-SR tapering $\alpha_{LT,F}-$ eq. (14)	155	0.99	0.030	1.05	0.90
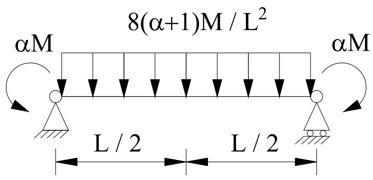	LBA-SR $C_{m,LT}$ approach	310	1.00	0.018	1.04	0.95
	LBA-SR tapering $\alpha_{LT,F} = 1.4\alpha_{LT}$	159	0.97	0.026	1.03	0.91
	LBA-SR tapering $\alpha_{LT,F}-$ eq. (14)	159	0.98	0.020	1.03	0.90
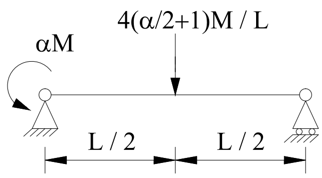	LBA-SR $C_{m,LT}$ approach	272	1.00	0.019	1.06	0.93
	LBA-SR tapering $\alpha_{LT,F} = 1.4\alpha_{LT}$	128	0.98	0.024	1.03	0.91
	LBA-SR tapering $\alpha_{LT,F}-$ eq. (14)	128	0.99	0.021	1.03	0.91
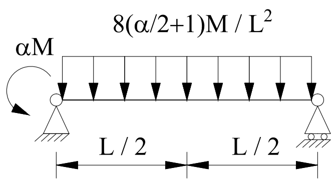	LBA-SR $C_{m,LT}$ approach	264	0.99	0.029	1.04	0.90
	LBA-SR tapering $\alpha_{LT,F} = 1.4\alpha_{LT}$	138	0.97	0.021	1.03	0.90
	LBA-SR tapering $\alpha_{LT,F}-$ eq. (14)	138	0.98	0.019	1.03	0.90
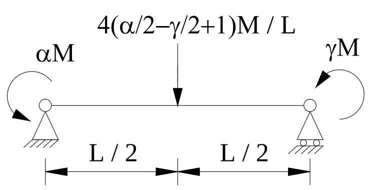	LBA-SR $C_{m,LT}$ approach	165	1.00	0.020	1.05	0.95
	LBA-SR tapering $\alpha_{LT,F} = 1.4\alpha_{LT}$	107	0.98	0.020	1.03	0.92
	LBA-SR tapering $\alpha_{LT,F}-$ eq. (14)	107	0.98	0.019	1.03	0.92

continued on next page

continued from previous page

Load case	Analysis approach	N	S_{av}	S_{cov}	S_{max}	S_{min}
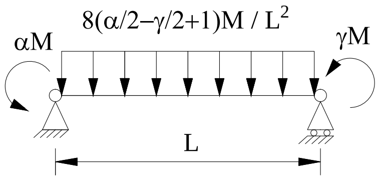	LBA-SR $C_{m,LT}$ approach	178	1.00	0.021	1.04	0.95
	LBA-SR tapering $\alpha_{LT,F} = 1.4\alpha_{LT}$	115	0.97	0.018	1.02	0.92
	LBA-SR tapering $\alpha_{LT,F}$− eq. (14)	115	0.97	0.017	1.02	0.92
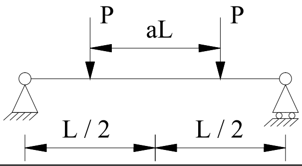	LBA-SR $C_{m,LT}$ approach	118	1.00	0.018	1.05	0.95
	LBA-SR tapering $\alpha_{LT,F} = 1.4\alpha_{LT}$	88	0.97	0.026	1.03	0.90
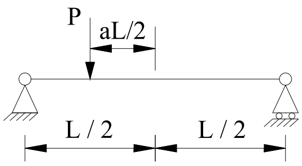	LBA-SR $C_{m,LT}$ approach	92	1.00	0.015	1.05	0.96
	LBA-SR tapering $\alpha_{LT,F} = 1.4\alpha_{LT}$	51	0.98	0.023	1.03	0.94